Available online at www.sciencedirect.com

SciVerse ScienceDirect

journal homepage: www.elsevier.com/locate/he

Experimental and numerical studies of the effects of hydrogen addition on the structure of a laminar methane–nitrogen jet in hot coflow under MILD conditions

Alexey Sepman [a,*], *Ebrahim Abtahizadeh* [b], *Anatoli Mokhov* [a], *Jeroen van Oijen* [b], *Howard Levinsky* [a,c], *Philip de Goey* [b]

[a] *Faculty of Mathematics and Natural Sciences, Energy and Sustainability Research Institute Groningen, University of Groningen, 9747 AG Groningen, The Netherlands*

[b] *Combustion Technology, Mechanical Engineering, Eindhoven University of Technology, 5600 MB Eindhoven, The Netherlands*

[c] *KEMA Nederland B.V., P.O. Box 2029, 9704 CA Groningen, The Netherlands*

ARTICLE INFO

Article history:
Received 15 May 2013
Received in revised form
22 July 2013
Accepted 3 August 2013
Available online 2 September 2013

Keywords:
Hydrogen addition
MILD combustion
Laminar flame
Laser induced fluorescence

ABSTRACT

In this work we investigate the effects of hydrogen addition on the flame structure of MILD combustion both experimentally and numerically using a laminar-jet-in-hot-coflow (LJHC) geometry. The addition of hydrogen appreciably decreases the flame height (~25%), however only modestly affects the maximal flame temperature and the thickness of combustion zone. The NO distribution is dominated by mixing of the NO formed in the coflow with the reaction products of the diluted fuel, with negligible NO formation from the fuel in all flames studied. The numerical data are in reasonably good agreement with the measurements.

1. Introduction

MILD (moderate and intense low-oxygen-dilution) combustion is a new technology combining high efficiency and low pollutant emissions in industrial heating processes [1]. This method adopts highly preheated and diluted air and/or fuel to homogenize the temperature field and minimize NO_x emission during combustion processes. An important aspect essential for successful implementation of this combustion technology is the robustness of a practical system to variations in fuel composition; under industrial conditions, fuels may vary from natural gas to H_2/CO mixtures containing unsaturated hydrocarbons, and the combustion systems must continue to operate within the desired performance envelope. Currently, there are relatively few studies considering variations in fuel composition on MILD combustion. For example, it was shown in [2] that adding ethane or N_2 to methane both widened the operating range for MILD combustion as

* *Corresponding author*. Laboratory for High Temperature Energy Conversion Processes, University of Groningen, 9747 AG Groningen, The Netherlands. Tel.: +31 50 3634759; fax: +31 50 3634479.
E-mail address: a.v.sepman@hotmail.com (A. Sepman).

0360-3199/$ – see front matter
http://dx.doi.org/10.1016/j.ijhydene.2013.08.015

compared to methane itself. Another study [3] found that the addition of N_2 or CO_2 to the fuel (a variety of fuel mixtures using methane, ethylene, and propane were investigated) reduced the NO_x emissions and facilitated flameless oxidation. In [4] it was reported that NO_x emissions are not sensitive to the hydrogen concentration under MILD conditions. A higher fuel jet velocity was required to achieve the transition from the conventional flame structure to MILD combustion when using a hydrogen–methane fuel [5] compared to pure methane, but a lower furnace temperature could be used. Only few studies considered the physical/chemical origins of the effects of fuel composition, in particular H_2 addition, on either the stability of the MILD regime or NO formation. For example, it was shown both computationally and experimentally in [6] that the reaction zone structure is very similar for the different fuels considered when hydrogen is added to the fuel stream. Hydrogen was found necessary for the experimental flames to stabilize. A numerical study [7] demonstrated that the hydrogen addition to methane leads to improved mixing, an increase in the turbulent kinetic energy decay along the flame axis and flame entrainment, higher reaction intensities, improved mixture ignitability and enhanced rate of heat release. Numerical and experimental investigations of burners operating in MILD combustion regime and fed with methane and methane–hydrogen mixtures showed the need of a detailed chemistry approach [8] and the need of a proper turbulence/chemistry interaction treatment [9] to capture the volumetric features of MILD combustion. The effect of the composition of methane/hydrogen mixture on mild flameless combustion was studied in [10] on a laboratory-scale facility. In [11] it was shown that hydrogen oxidation kinetic significantly interacts with methane Mild Combustion process. See also [12] for more references on the flameless oxidation of various fuels. We note that all above mentioned work was done in turbulent flames. To our knowledge there are no combined experimental and numerical studies of the effects of fuel composition on MILD flames in good defined conditions where chemical models can be tested.

In this work we investigate the effects of hydrogen addition on both spatial structure and the NO formation of a MILD flame burning using an axisymmetric laminar-jet-in-hot-coflow (LJHC) burner both experimentally and numerically. Towards this end, we expand our previous studies performed on the MILD flame with methane as a basis fuel (this base flame was investigated by the authors in [13–15]) by adding hydrogen to the fuel. The distributions of temperature and fractions of major species and NO are measured using spontaneous Raman scattering and laser-induced fluorescence (LIF).

2. Experimental

A schematic of the LJHC burner is shown in Fig. 1. An upright ceramic fuel tube (i.d. of 7 mm, wall thickness of 1.5 mm) was surrounded by a coflow annulus (a perforated ceramic tile with an overall diameter of 58 mm). The experimental conditions (the exit velocity, temperature and composition) for the fuel and oxidizer are reported in Table 1 for two Cases studied. The hot oxidizer stream was formed by the combustion products of a nearly one-dimensional flame of a fuel-lean $N_2/CH_4/O_2$ mixture, see [14,15] for more details on the operation of the burner. The experimental and numerical results for Case M were reported and thoroughly described in our previous works [13–15]. Here we study the effects of the H_2 addition to the fuel on the spatial structure of the MILD flame (Case M). Methane and hydrogen were mixed while keeping the total flow rate of the fuel constant. The flows of all gases were measured using calibrated mass flow meters (Bronkhorst). The velocities reported in Table 1 are the flows of coflow and fuel (measured at standard conditions) normalized by the corresponding exit areas. The profiles of temperature and species fractions were obtained by moving the burner axially and radially (vertically and horizontally, respectively) by a precision positioner (Parker, positioning uncertainty less than 0.1 mm).

The flame temperature, major species (CO, CO_2, N_2, H_2, H_2O, CH_4 and O_2) and NO fractions were measured using spontaneous Raman scattering and Laser induced Fluorescence, respectively. The optical scheme for the spontaneous Raman measurements is essentially identical to that described in [16]. At the exit plane of an f/4 Acton Research Spectra Pro 2300i spectrometer, a PI-Max intensified 1024 × 1024 pixel CCD camera (Princeton Instruments, 13 μm pixel size) was mounted. In the present study, 40 pixels were binned along the axis of the laser beam, integrating the signal over distances of roughly 1 mm, yielding the radial spatial resolution of the experiment. The temperature measurements were performed using moderately resolved Raman spectra of N_2, the concentration measurements using low-resolution Raman spectra which included the spectral features of all

Table 1 – The experimental conditions.

Case	Coflow							Fuel				
	v^a (cm/s)	$O_2{}^b$	N_2	H_2O	CO_2	NO (ppm)	T^c (K)	v^a (cm/s)	CH_4	H_2	N_2	T^d (K)
M	15.5	0.036	0.732	0.145	0.087	10	1530	5.8	0.18		0.82	1150
H	15.5	0.036	0.732	0.145	0.087	10	1530	5.8	0.09	0.09	0.82	1185

a The exit velocities are reported at Standard conditions ($T = 273$ K, $P = 1$ atm).
b The composition of gases is given by volume %.
c Coflow temperature in the exit plane of the fuel tube.
d Fuel temperature at 3 mm above the exit plane of the fuel tube.

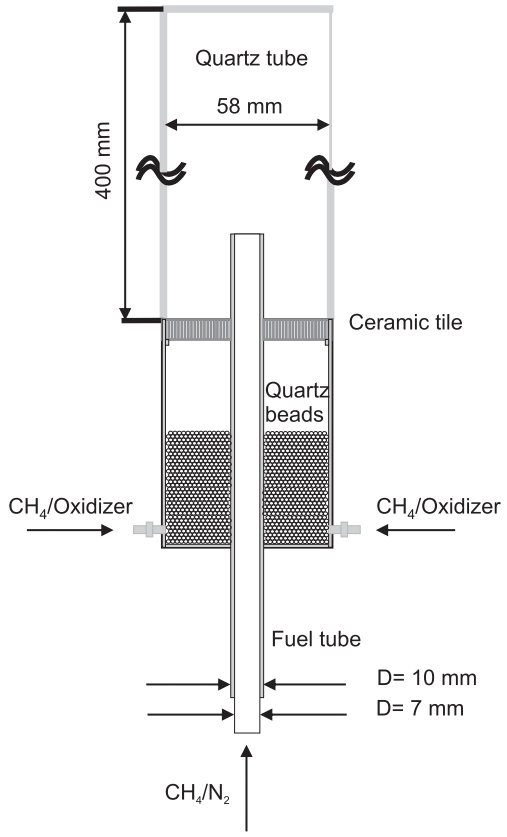

Fig. 1 – Schematic of the laminar-jet-in-hot-coflow burner.

major species in our flames. The optical scheme of the LIF measurements and the method to derive the absolute NO concentration are described elsewhere [14] and in its references. In brief, a Sirah PrecisionScan tunable dye laser pumped by the second harmonic of a Spectra-Physics Quantra Ray Pro 250-10 *Nd:YAG* laser was used to generate wavelengths near 226 nm, with pulse duration $\tau \sim 10$ ns, by mixing the dye output with the third harmonic of the same laser. The laser beam was focused to the flame by a quartz lens ($f = 85$ cm). The laser pulse energies were typically less than 10 μJ to assure linearity of the LIF signals. Fluorescence from the centre of the flame was collected at right angles by a quartz lens (Nikkor f/4.5) and focused onto an Acton Research Corporation SpectraPro 2150i spectrometer (f/4, 10 nm/mm). The spectrometer bandpass was set to 30 nm to capture the entire NO A-X(0, 3) band. The fluorescence signals were detected by an Electron Tubes 9659QB photomultiplier. The spatial resolution of the NO measurements along the laser beam in this work was ~1.5 mm.

3. Computations

The mathematical formulation and numerical methodology used to perform the modeling was extensively discussed in [15]. In short, the governing equations for mass, momentum, energy and species are written in the cylindrical coordinate system. The equations are solved using a finite-volume, density based, body-fitted multi-block quadrilateral mesh together with a parallel adaptive mesh refinement (AMR) following the approach developed in [17]. The Soret effect was not included in the calculations, see below. The numerical calculations were performed with the GRI-Mech 3.0 detailed chemical reaction mechanism [18]. The GRI-Mech 3.0 mechanism was adopted with some modification of the NO chemistry, see [19,20]. Namely, the reaction $CH + N_2 \rightarrow HCN + N$ in GRI 3.0 mechanism, is changed to

$$CH + N_2 \rightarrow NCN + H, \quad \text{(R1)}$$

while keeping the same rate constant, and 4 reactions describing the reactions of NCN with O, H, OH, O_2 are added:

$$NCN + O \rightarrow CN + NO \quad \text{(R2)}$$

$$NCN + H \rightarrow HCN + N \quad \text{(R3)}$$

$$NCN + OH \rightarrow HCN + NO \quad \text{(R4)}$$

$$NCN + O_2 \rightarrow NCO + NO \quad \text{(R5)}$$

The calculations were performed using rate coefficients for these four reactions taken from Lin and co-workers [21–24]; the values used are summarized in [19]. Transport is described by a mixture averaged model in which the diffusion velocity of each individual species is calculated assuming Fickian diffusion.

Here we investigate the importance of the Soret effect in the computations of Case H by comparing the chemical time scales of corresponding 1D igniting counterflow diffusion flame (see Fig. 2). These 1D flames are computed with the same composition and temperature of fuel and oxidizer of the Case H_2 using the GRI-Mech 3.0 and mixture-averaged multicomponent transport (details of computations can be found in [25]). ΔT represents the temporal evolution of temperature in mixture fraction space:

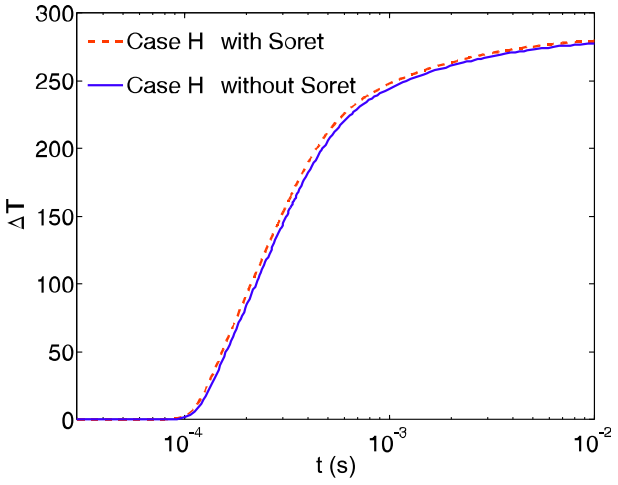

Fig. 2 – Influence of the Soret effects on the evolution of temperature during autoigni-tion of Case H obtained from computations of igniting counterflow diffusion flames.

$$\Delta T(t) = \max_{Z}(T(Z,t) - T(Z,0)) \quad (1)$$

A comparison of ΔT between the computations indicates that the contribution of the Soret effect to the predicted chemical time scales is less than 5%. Such a small contribution of the Soret effect in the 1D computations can be explained since this effect is only important for light species (H, H_2, He) at low temperatures [26]. Since the mass fraction of H_2 in the fuel stream is very small (0.0073) and the temperature levels are high (above 1000 K) eventually the contribution of the Soret effect is small in the studied conditions. This observation can be translated into the corresponding computed laminar 2D flames since the turbulence transport is absent and molecular diffusion plays an important role in the flame structure. In our previous study [15], it has been demonstrated that the structure of the 2D laminar Mild flames can be described very well with the computed 1D igniting flamelets. This is due to the autoignition structure of the Mild flame. A small change in the chemical time scales of the computed 1D flames can hardly influence the location of the maximum heat release and the flame structure of the computed 2D flames. Consequently, the Soret effect can be safely neglected in the 2D computations.

4. Results and discussion

4.1. General structure of flames

To illustrate the effects of hydrogen addition on the overall flame structure, we present two-dimensional false color plots of the computed distribution of temperature for flames with and without hydrogen addition in Fig. 3. The figure includes the stoichiometric and most reactive mixture fraction (see [15] and below) iso-contours. First of all, we note that the hydrogen addition does not affect the general flame appearance significantly. Indeed the extent of high temperature zone of two flames is comparable and the maximum temperatures are rather similar, being ~50 K higher in Case M. However, the addition does appreciably influence the position of the temperature rise in respect to the location of the burner outlet. The significant temperature rise in Case M is evident at a height of ~6 mm, while that in Case H is visible at a height of ~3 mm. Such a behavior indicates that the hydrogen addition promotes ignition. The location of the temperature rise in Case H is also somewhat shifted to the fuel side in comparison with that in Case M. We also note that the hydrogen addition decreases significantly the axial location of a stoichiometric contour from ~18 mm to 12 mm. The above comments are further illustrated by the simulated heat release rate distributions shown in Fig. 4 together with streamlines and the iso-contours. As can be seen from Figs. 3 and 4, the location of maximal temperature at every height corresponds to the position of the maximal heat release. Fig. 4 also shows that in both Cases the combustion starts at a lean mixture fraction, proceeds further downstream towards and beyond the stoichiometric mixture fraction. We further note that the both heat release profiles are notably different from those of coflow diffusion edge flames, see for examples [15]. This is due to the fact that the flame temperature in our Cases is not large enough to support an edge flame that can propagate upstream. Therefore, it can be concluded that stabilization mechanism of these cases is governed by autoignition.

The autoignition structure of Cases M and H is further analyzed by plotting the computed distributions of the production rate of formaldehyde in Fig. 5. It is clear that for both flames CH_2O is formed upstream of the maximum heat

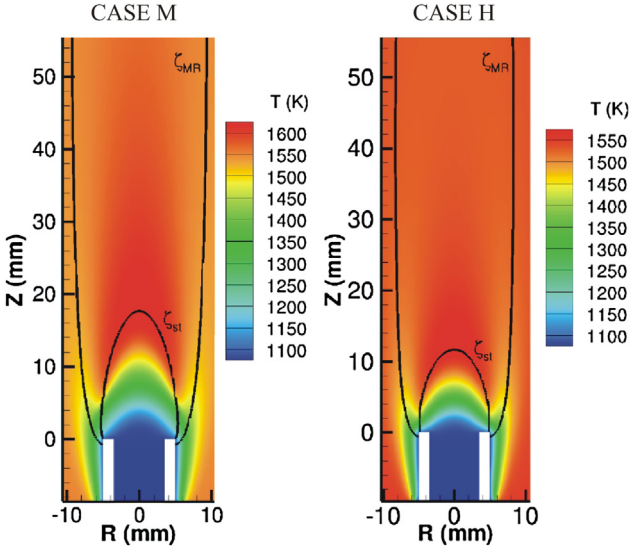

Fig. 3 – Two-dimensional false color plots of the line computed temperature in Cases M and H. The black lines show the stoichiometric, ζ_{st}, and most reactive mixture fraction, ζ_{MR}, iso-contours. (For interpretation of the references to color in this figure legend, the reader is referred to the web version of this article.)

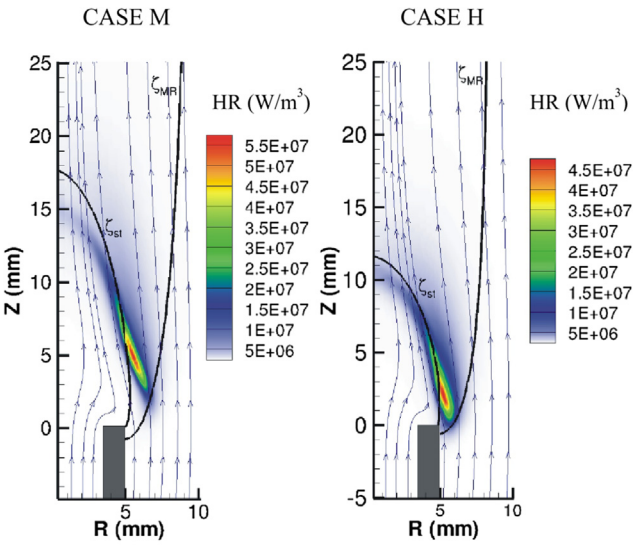

Fig. 4 – Two-dimensional false color plots of the computed heat release (HR) for Cases M and H. The lines with arrows represent streamlines of the velocity field. The black lines show the stoichiometric ζ_{st} and most reactive mixture fraction ζ_{MR} iso-contours. (For interpretation of the references to color in this figure legend, the reader is referred to the web version of this article.)

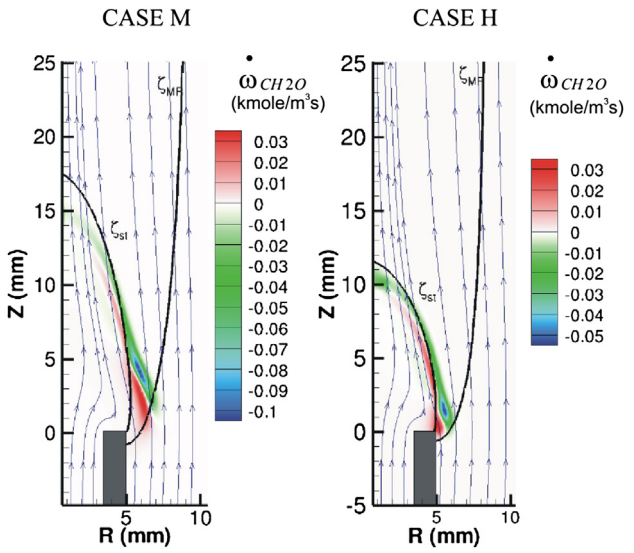

Fig. 5 – Two-dimensional false color plots of the computed production rate of formaldehyde ($\dot{\omega}(CH_2O)$) for Cases M and H. The lines with arrows represent streamlines of the velocity field. The black lines show the stoichiometric ζ_{st} and most reactive mixture fraction ζ_{MR} iso-contours. (For interpretation of the references to color in this figure legend, the reader is referred to the web version of this article.)

release location, immediately above the burner tip. The produced CH_2O is then consumed downstream at the maximum heat release location. We note that such a behavior is in a clear contrast with the trends that have been observed for the edge flames, see [15], where CH_2O is formed downstream of the maximum heat release and it is diffused upwards towards the maximum heat release location where it is consumed. This again demonstrates the stabilization of these flames by the autoignition phenomena. The location of the heat release and CH_2O production rate can be discussed in terms of most reactive mixture fraction ζ_{MR} (the mixture fraction with the shortest autoignition time) [27]. This value has been obtained from the computations of a homogeneous reactor for various frozen mixtures of fuel and oxidizer in a 1D configuration for Cases M and H (more details can be found in [25] and [15]). It is observed that ignition starts from ζ_{MR} similar to what has been reported for the autoignition structures [25,27,28]. The ζ_{MR} is located at the lean side due to the higher temperature and availability of a small amount of O_2 at the coflow side.

Figs. 3–5 also display the increased diffusivity of the mixture due to hydrogen addition. Indeed, since the methane and hydrogen were mixed while keeping the total flow rate of the fuel constant, the global equivalence ratio has decreased by the hydrogen addition. However, the position of the stoichiometric mixture fraction contour near the burner outlet is practically not affected by the hydrogen addition.

An important aspect of Case H compared to Case M is the flame stability which is significantly improved by H_2 enrichment. In fact, auto-ignition of these flames is initiated at low mixture fractions (<0.12) close to coflow stream in localized regions of low scalar dissipation rate. Preferential diffusion effects of H_2 leads to an increased presence of fuel at this most reactive mixture fraction [29] and eventually an increased chemical reactivity and stability of the flame. This observation corresponds very well with recent measurements of the turbulent Jet-in-Hot Coflow burner of TU Delft [30]. In these measurements, they have added a range 5%–25% hydrogen to the lifted Mild flames and they have observed a significant improvement in stability together with shorter lift-off height. Also the works of the Adelaide group [6] confirm that the flame stabilization in MILD combustion is very similar for different fuels (NG, C_2H_4 and LPG) with H_2 enrichment. Such an improvement in the flame stability induced by the presence of hydrogen suggests a more flexible range of possible fuels for application in MILD combustors.

To supplement the computational findings as to the effect of the H_2 addition on the flame structure, we compare the radial profiles of temperature measured at 3 and 12 mm above the burner outlet for two cases studied in Fig. 6. To illustrate the development of the flames, we plot the difference between the radial profiles measured in flames with those measured when only N_2 was flowing through the fuel tube. The situation when only N_2 is present in the fuel tube corresponds to frozen (no chemical activity) mixing between coflow and fuel. The development in the profiles of the temperature difference for both flames reflect the "wishbone-shaped" radial temperature distributions in an "ordinary" diffusion flame [15], with the exception that the temperature rise in non-diluted coflow is approximately a factor of 9 higher than that shown in Fig. 6. The figure shows that at 3 mm height the peak in the temperature difference in Case M is ~100 K, while that in Case H it is ~200 K. The experimental data at 3 mm height show the presence of a noteworthy measured amount of O_2 near the centerline in Case M [15], while in Case H the O_2 mole fraction

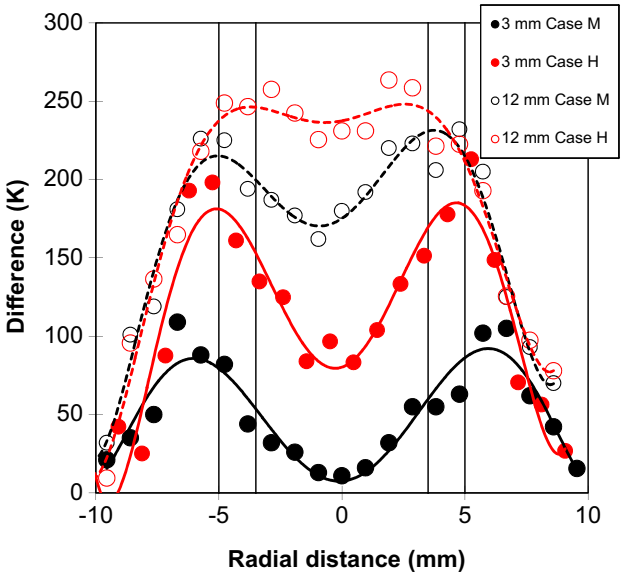

Fig. 6 – The differences between the radial temperature profiles at 3 and 12 mm with those measured when only N_2 was flowing through the fuel tube. High-order polynomial trendlines are added to accentuate the trends in the experimental data.

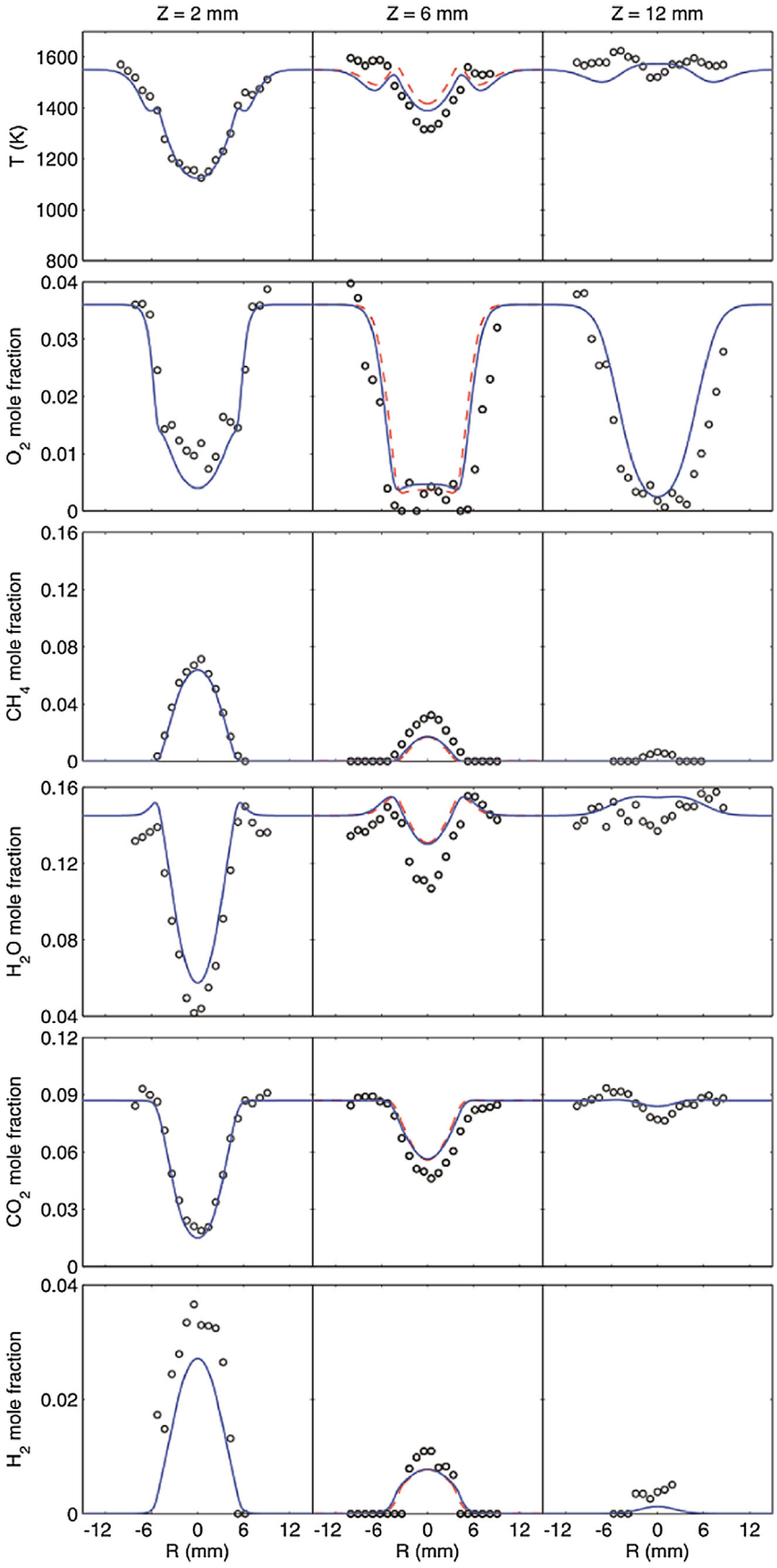

Fig. 7 – Measured (pointes) and computed (lines) radial profiles of temperature and major species in Case H. Red dash lines denote the calculations with a considerably reduced thickness of the thermal boundary layer. (For interpretation of the references to color in this figure legend, the reader is referred to the web version of this article.)

is close to zero (not shown), similarly to the data at 2 mm (see Fig. 7). The analysis of the data measured in the vicinity of the burner outlet indicated that the hydrogen addition promotes the ignition. We would like also to mention that the radial profiles of the temperature difference in Case M measured at several downstream distances, see Fig. 6 and [13] show the peak in the temperature difference on the level of 200 K. This value is similar to those for Case H. The figure also shows that the position of the maximal heat release shifts notably towards the burner outlet with the addition. We would like to note that some of the described above effects of the hydrogen addition on general flame structure such as reduction of the flame height and the shift of the reaction zone towards the burner exit were also reported in [8].

4.2. *Comparison of the experimental results measured in Case H with the numerical simulations*

As an example of the measurements performed, Fig. 7 shows the experimental radial profiles of temperature and major species mole fractions at the axial distances 2, 6 and 12 mm in Case H. To test the predictive power of the GRI 3.0 mechanism at the specific experimental conditions, we contrast the measurements with the results of the computation. The progress of combustion in Case H is reflected in the development of temperature. However the details of the evolution is considerably masked by the large temperature difference between the coflow and fuel similarly as in the flame without hydrogen addition (Case M), see [13,15]. The development of the major species profiles for Case H is consistent with temperature changes. The experimental temperature agrees quantitatively with the computations at the axial distance of 2 mm. We note that the little bump in the experimental temperature profile (marking apparently the location of combustion zone) at the radial distance of ~5 mm is well captured. At the axial distances of 6 and 12 mm, the agreement is also good, the calculations predict the measured data within 120 K and generally better. The calculations predict rather well the H_2 profiles and somewhat overpredict the CH_4 consumption. The O_2 profile is quantitatively predicted at the height of 2 mm. We noted already the presence of significant amount of O_2 near the centerline. Further downstream, however, the decrease in the experimental O_2 fraction at the edges of the measured domain occurs notably closer (~1.5 mm) to the coflow side than that in calculations. Such a behavior implies that the computational combustion zone is shifted in comparison with the experimental one closer to the fuel side. The overprediction of CO_2 and H_2O profiles inside the domain of the fuel flow for some axial distances is consistent with this shift.

Fig. 8 shows the experimental and calculated vertical profiles of T and CH_4 and H_2 mole fractions. The experimental temperature rapidly increases to the maximum temperature of ~1580 K, at the distance of ~15 mm above the burner outlet. The computations support the maximum measured temperature quantitatively, however, approach it faster and reach the maximum already at a distance of ~12 mm. In accordance with the observed difference in the behavior of the temperature profiles, the calculations and measurements show similar discrepancy in the fuel profiles. While the

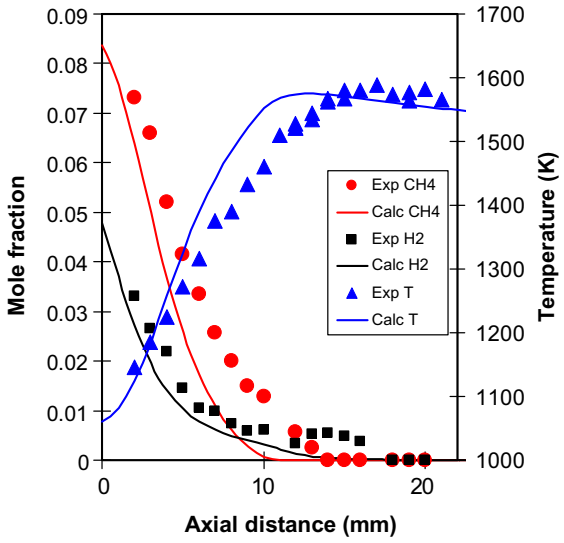

Fig. 8 – The experimental and calculated vertical profiles of temperature and CH_4 and H_2 mole fractions in Case H.

experimental data demonstrate the non-negligible CH_4 and H_2 mole fractions at distances above 12 mm, the computations show that all fuel is consumed by a height of 12 mm. The rapid initial decrease in the vertical CH_4 and H_2 profiles is a result of the diffusion of fuel in radial directions towards the flame front. We would like to point out to the interesting feature, qualitatively well captured also by the calculations, in behavior of the vertical CH_4 and H_2 profiles in the vicinity of the maximal heat release. The CH_4 concentration is consumed rapidly in the fuel-rich part of the flame front (see also Fig. 9), while most of the H_2 concentration survives this region; the hydrogen burns out completely further downstream at the stoichiometric and fuel lean conditions. The behavior is not perhaps unexpected, the one-dimensional flame calculations of the CH_4/H_2 blends demonstrate that a significant part of the

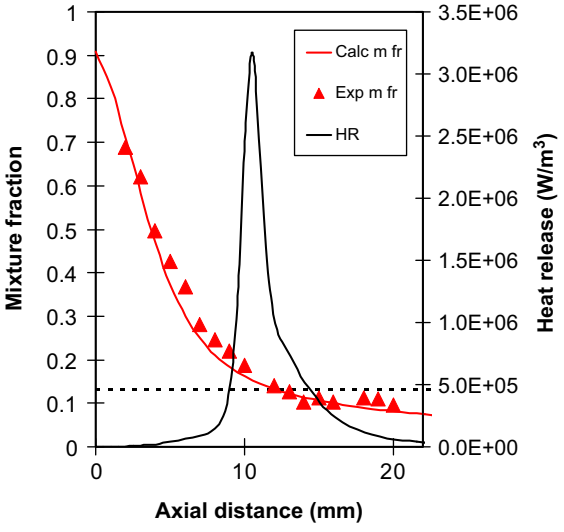

Fig. 9 – The vertical profiles of mixture fraction and heat release (HR) in Case H (symbols: measurements, lines: computations). The horizontal line marks the position of stoichiometric mixture fraction.

hydrogen is not consumed at fuel-rich conditions. Fig. 9 shows the vertical profiles of heat release and the mixture fractions. The mixture fraction was calculated using Bilger's formula [31] modified to account for the presence of C and H in the oxidizer. The horizontal line in Fig. 9 marks the position of stoichiometric mixture fraction. Here we point out that the mixture fraction is predicted well, but the CH_4 and H_2 profiles are less accurately reproduced (Fig. 8).

Although the computations in Case H reproduce quite well the general trend of the experimental data, the results of this section indicated some quantitative differences. The examination of the behavior of the experimental and calculated profiles suggests that the computational flame burns faster than the experimental one.

A possible reason for the differences might be the choice of the boundary conditions. Namely, in Cases M and H, the thermal boundary layer between the fuel tube and the coflow was chosen in a way to reproduce the measured values of temperature for the non-reacting mixture [15]. To do this, CH_4 has been completely removed and replaced by N_2, keeping all other parameters of the Case M the same, to avoid any possible heat release. The calculated temperature corresponded very well with the measured values at a height of 3 mm and 12 mm above the fuel tube exit and further modeling of Case M provided a very good match with the experimental data. In [15], however, we did not check the sensitivity of the numerical results to the chosen boundary conditions. In an attempt to analyze the sensitivity, we also performed the numerical calculations with a considerably reduced thickness of the thermal boundary layer (see [15]). Fig. 7 includes the radial profiles of temperature and species concentrations calculated using these new boundary conditions at a height of 6 mm. The figure shows that decreasing the boundary layer thickness does not affect significantly both the temperature and species distributions.

While we can not exclude other possible reasons for the differences observed (for example, uncertainties in kinetics and transport, or uncertainty in vertical position), we believe that a further analysis of the physical/chemical reasons would hardly be justified and is beyond the scope of the manuscript. We are also of the opinion that such an analysis would require an addition experimental efforts, perhaps, the measurements of the OH radical distribution might be beneficial for this purpose (we plan to conduct such measurements in the future). Furthermore, there may not exist a single reason which explains these differences.

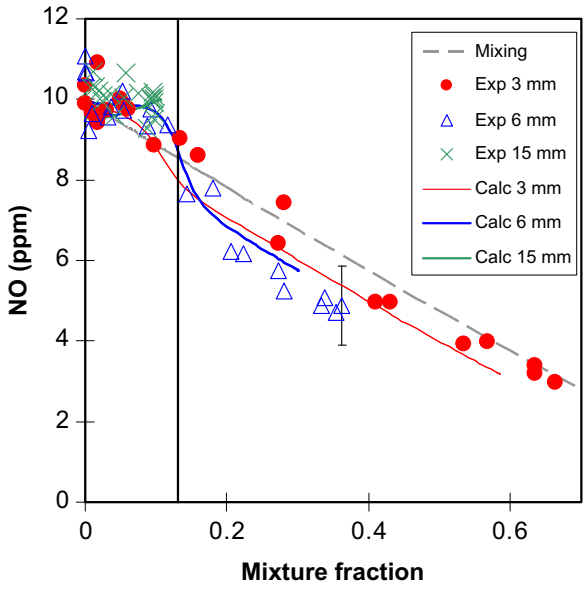

Fig. 11 – Measured and calculated NO mole fractions versus mixture fraction in Case H. The vertical line marks the position of stoichiometric mixture fraction.

4.3. *The NO formation in CH_4/H_2 flame*

Fig. 10 displays the NO radial profiles measured and calculated at axial positions of 3, 6 and 15 mm in Case H. At the axial distances of 3 and 6 mm the NO profiles show a minimum at the flame centre, at 15 mm the profile becomes flat. Comparison with the calculated profiles shows excellent agreement. We remind here that a similar trend in the behavior of the NO radial profile with downstream distance was noticed in Case M [13,14]. In these papers it was also found (by analyzing the experimental and computational data in mixture fraction space) that the NO field is dominated by mixing of the NO formed in the coflow with the reaction products of the diluted fuel, with negligible NO formation from the fuel via the Fenimore mechanism. To check the effects of H_2 addition on the NO formation, we plot the experimental and computational results as a function of

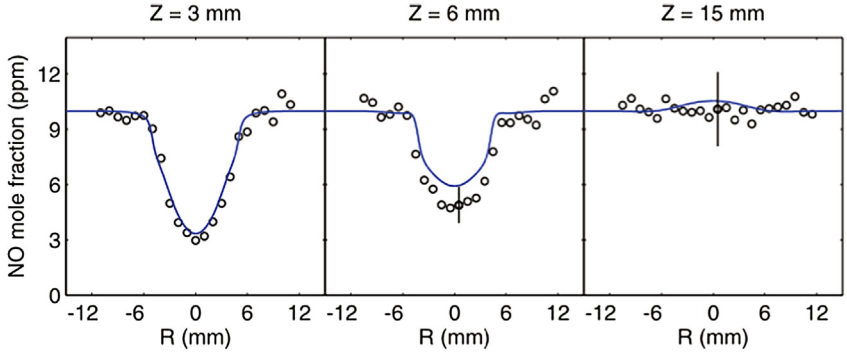

Fig. 10 – The measured and calculated radial profiles of NO in Case H at axial positions of 3, 6 and 15 mm. Pointes denote measurements; lines denote calculations.

mixture fraction in Case H, see Fig. 11. The figure also includes the mixing curve indicating simple mixing of the hot coflow with the combustion products of the fuel jet, $(NO) = (1 - \zeta)(NO)_{ox}W_M/W_{ox}$, where ζ is the mixture fraction, $(NO)_{ox}$ is NO fraction in the oxidizer (10 ppm) and W_M and W_{ox} are molecular weights of the combustion products at the measuring position and oxidizer stream, respectively. The measurements and calculations at 3 and 15 mm cluster around the mixing curve demonstrating almost no NO formation or consumption. The comparison of the measured NO fraction at 6 mm with the mixing line demonstrates a noticeable NO consumption at the fuel rich conditions, the difference is on the level ~30%, clearly outside the measurement uncertainty of 20%. We note that in Case M at the given level of the NO seeding in the coflow, the difference was on the level of 20%. At the fuel lean side the date concentrate around the mixing line. The calculations support the measurements quantitatively, although they predict a somewhat smaller difference with the mixing line (~20%) at fuel rich conditions. The rate-of-production analysis reveals that the consumption is mostly due to the conversion of the NO molecules to the N-containing intermediates (HCN, NH_3 and HNCO). These intermediates (similarly to Case M) are converted back to NO at downstream distances.

5. Conclusions

An experimental and computational study of the effects of the H_2 addition on both the spatial structure and the NO formation of a MILD flame burning in an axisymmetric laminar-jet-in-hot-coflow geometry has been performed. Using methane as base fuel, the effects of adding H_2 were studied. The addition of hydrogen appreciably decreases the flame height (~25%) and promotes the ignition, however only modestly affects the maximal flame temperature and the thickness of combustion zone. The numerical data are in reasonably good agreement with the measurements. Analysis of the NO fraction as a function of mixture fraction indicates that the NO distribution is dominated by mixing of the NO formed in the coflow with the reaction products of the diluted fuel, with negligible NO formation from the fuel in all flames studied. Experiments show the considerable reduction of the seeded NO at a height of 6 mm. The calculations support the observation quantitatively and reveal that the reduction is due to the conversion of the NO molecules to the N-containing intermediates which are converted back to NO at downstream distances.

Acknowledgments

We gratefully acknowledge support from the Dutch Technology Foundation (STW) for this work within the framework of the Clean Combustion Concepts (CCC) program.

REFERENCES

[1] Cavaliere A, de Joannon M. Mild combustion. Prog Energy Combust Sci 2004;30(4):329–66.
[2] Effuggi A, Gelosa D, Derudi M, Rota R. Mild combustion of methane-derived fuel mixtures: natural gas and biogas. Combust Sci Technol 2008;180(3):481–93.
[3] Dally BB, Riesmeier E, Peters N. Effect of fuel mixture on moderate and intense low oxygen dilution combustion. Combust Flame 2004;137(4):418–31.
[4] Yu Y, Gaofeng W, Qizhao L, Chengbiao M, Xianjun X. Flameless combustion for hydrogen containing fuels. Int J Hydrogen Energy 2010;35(7):2694–7.
[5] Derudi M, Villani A, Rota R. Mild combustion of industrial hydrogen-containing byproducts. Ind Eng Chem Res 2007;46(21):6806–11.
[6] Medwell PR, Dally BB. Effect of fuel composition on jet flames in a heated and diluted oxidant stream. Combust Flame 2012;159(10):3138–45.
[7] Mardani A, Tabejamaat S. Effect of hydrogen on hydrogen-methane turbulent non-premixed flame under MILD condition. Int J Hydrogen Energy 2010;35(20):11324–31.
[8] Parente A, Galletti C, Tognotti L. The MILD combustion in an industrial burner fed with hydrogen enriched fuels. Int J Hydrogen Energy 2008;33:7553–64.
[9] Galletti C, Parente A, Derudi M, Rota R, Tognotti L. Numerical and experimental analysis of NO emissions from a lab-scale burner fed with hydrogen-enriched fuels and operating in MILD combustion. Int J Hydrogen Energy 2009;34:8339–51.
[10] Ayoub M, Rottier C, Carpentier S, Villermaux C, Boukhalfa AM, Honore D. An experimental study of mild flameless combustion of methane/hydrogen mixtures. Int J Hydrogen Energy 2012;37:6912–21.
[11] Sabia P, de Joannon M, Fierro S, Tregrossi A, Cavaliere A. Hydrogen-enriched methane Mild Combustion in a well stirred reactor. Exp Thermal Fluid Sci 2007;31:469–75.
[12] Verissmo AS, Rocha AMA, Costa M. Operational, combustion, and emission characteristics of a small-scale combustor. Energy Fuels 2011;25:2469–80.
[13] Sepman AV, Mokhov AV, Levinsky HB. Spatial structure and NO formation of a laminar methane-nitrogen jet in hot coflow under MILD conditions: a spontaneous Raman and LIF study. Fuel 2013;103:705–10.
[14] Sepman AV, Abtahizadeh SE, Mokhov AV, van Oijen JA, Levinsky HB, de Goey LPH. Numerical and experimental studies of the NO formation in laminar coflow diffusion flames on their transition to MILD combustion regime. Combust Flame 2013;160:1364–72.
[15] Abtahizadeh E, Sepman AV, van Oijen J, Mokhov AV, de Goey P, Levinsky HB. Numerical and experimental investigations on the influence of preheating and dilution on transition of laminar coflow diffusion flames to "MILD" combustion regime. Combust Flame 2013. in press.
[16] Sepman AV, Toro VV, Mokhov AV, Levinsky HB. Determination of temperature and concentrations of main components in flames by fitting measured Raman spectra. Appl Phys B 2013;112:35–47.
[17] Groth CPT, De Zeeuw DL, Gombosi TI, Powell KG. A parallel adaptive 3D MHD scheme for modeling coronal and solar wind plasma flows. Space Sci Rev 1999;87(1–2):193–8.
[18] Smith GP, Golden DM, Frenklach M, Moriarty NW, Eiteneer B, Goldenberg M, et al. <http://www.me.berkeley.edu/gri_mech/>.
[19] Sepman AV, Mokhov AV, Levinsky HB. The effects of hydrogen addition on NO formation in atmospheric-pressure, fuel-rich-premixed, burner-stabilized methane, ethane and propane flames. Int J Hydrogen Energy 2011;36(7):4474–81.
[20] Sepman AV, Mokhov AV, Levinsky HB. The effects of the hydrogen addition on the HCN profiles in fuel-rich-

premixed, burner-stabilized C1-C3 alkane flames. Int J Hydrogen Energy 2011;36(21):13831–7.
[21] Moskaleva LV, Lin MC. The spin-conserved reaction CH + N_2 → H + NCN: a major pathway to prompt NO studied by quantum/statistical theory calculations and kinetic modeling of rate constant. Proc Combust Inst 2000;28:2393–401.
[22] Zhu RS, Lin MC. Ab initio study of the oxidation of NCN by O_2. Int J Chem Kinet 2005;37(10):593–8.
[23] Zhu RS, Lin MC. Ab initio study on the oxidation of NCN by O (P-3): prediction of the total rate constant and product branching ratios. J Phys Chem A 2007;111(29):6766–71.
[24] Zhu RS, Nguyen HMT, Lin MC. Ab initio study on the oxidation of NCN by OH: prediction of the individual and total rate constants. J Phys Chem A 2009;113(1):298–304.
[25] Abtahizadeh E, van Oijen J, de Goey P. Numerical study of Mild combustion with entrainment of burned gas into oxidizer and/or fuel streams. Combust Flame 2012;159(6):2155–65.
[26] Warnatz J, Mass U, Dibble RW. Combustion. Springer; 1996.
[27] Mastorakos E. Ignition of turbulent non-premixed flames. Prog Energy Combust Sci 2009;35(1):57–97.
[28] Sorrentino G, Scarpa D, Cavaliere A. Transient inception of MILD combustion in hot diluted diffusion ignition (HDDI) regime: a numerical study. Proc Combust Inst 2013;34(2):3239–47.
[29] van Oijen JA. Prog Combust Inst 2013;34(1):1163–71.
[30] Arteaga Mendez LD, Tummer MJ, Roekaerts DJEM. Effect of hydrogen on the stabilization mechanism of natural gas jet-in-hot-coflow flames. In: Proc 6th Eur Combust Meet 2013P1–16.
[31] Bilger RW, Starner SH, Kee RJ. On reduced mechanisms for methane air combustion in nonpremixed flames. Combust Flame 1990;80(2):135–49.